

EARTHSCAN REFERENCE COLLECTIONS

RENEWABLE ENERGY

VOLUME II

RENEWABLE ENERGY TECHNOLOGIES

I

EDITED BY
BENT SØRENSEN

earthscan

EARTHSCAN REFERENCE COLLECTIONS

Renewable Energy

Volume II

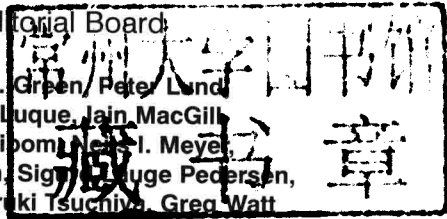
Renewable Energy Technologies I

Edited by

Bent Sørensen

Editorial Board

Martin A. Green, Peter Lund,
Antonio Luque, Jain MacGill,
Peter Meibom, Neil I. Meyer,
Walt Patterson, Sigurd Lauge Pedersen,
Ari Rabl, Haruki Tsuchiya, Greg Watt



earthscan

publishing for a sustainable future

London • Washington, DC

First published in 2011 by Earthscan

Editorial material and selection copyright © Bent Sørensen 2011

Copyright for individual chapters is indicated in a footnote on the opening page of each chapter

All rights reserved. No part of this publication may be reproduced, stored in a retrieval system, or transmitted, in any form or by any means, electronic, mechanical, photocopying, recording or otherwise, except as expressly permitted by law, without the prior, written permission of the publisher.

The editor and publisher gratefully acknowledge the permission granted to reproduce the copyright material in this book. Every effort has been made to trace copyright holders and to obtain their permission for the use of copyright material. The publisher apologizes for any errors or omissions and would be grateful if notified of any corrections that should be incorporated in future reprints or editions of this book.

Earthscan Ltd, Dunstan House, 14a St Cross Street, London EC1N 8XA, UK
Earthscan LLC, 1616 P Street, NW, Washington, DC 20036, USA

Earthscan publishes in association with the International Institute for Environment and Development

For more information on Earthscan publications, see www.earthscan.co.uk
or write to earthinfo@earthscan.co.uk

ISBN: 978-1-84407-867-7

Typeset by Domex e-Data, India
Cover design by Andrew Corbett

A catalogue record for this book is available from the British Library

Library of Congress Cataloging-in-Publication Data

Sørensen, Bent, 1941–

Renewable energy / Bent Sørensen.

4 v. cm.

Includes bibliographical references and index.

ISBN 978-1-84407-867-7 (hardback)

1. Renewable energy sources. I. Title.

TJ808.S66 2011

621.042–dc22

2010045201

At Earthscan we strive to minimize our environmental impacts and carbon footprint through reducing waste, recycling and offsetting our CO₂ emissions, including those created through publication of this book. For more details of our environmental policy, see www.earthscan.co.uk.

Printed and bound in the UK by CPI Antony Rowe.
The paper used is FSC certified.



Renewable Energy

Volume II

List of Abbreviations

Å	angstrom (10^{-10} m)
AFM	atomic force microscopy
a-Ge	amorphous germanium
AR	antireflection coating
a-Si	amorphous silicon
ATES	aquifer thermal energy store
ATR-FTIR	attenuated total reflectance–Fourier transform infrared
BAPV	building-applied photovoltaics
BIPV	building-integrated photovoltaics
BOS	balance-of-systems
BTES	borehole thermal energy store
Btu	British thermal unit (1055J)
CB	conduction band
CDI	carrier density imaging
CEC	Commission of the European Communities
CNRS	Centre National de la Recherche Scientifique (National Center of Scientific Research)
C-PCM	conductor-like polarizable continuum model
CSHPSS	central solar heating plants with seasonal heat storage
CSU	Colorado State University
Cz	Czochralski
DC	direct current
DEZ	diethylzinc
DFT	density functional theory
DSG	direct steam generation
EBIC	electron-beam-induced current
EDT	1,2-ethanedithiol
EMF	electromotive force
EPD	etch pit density
EQE	external quantum efficiency
ERDA	Energy Research and Development Administration
eV	electron volt
FCV	fuel cell vehicle
FET	field effect transistor

FF	fill factor
ft	foot (0.3m)
FZ	float zone
GWTES	gravel-water thermal energy store
HFCV	hybrid fuel cell vehicle with regenerative braking
HFCVP	hybrid fuel cell vehicle with regenerative braking and rooftop PV
HOMO	highest occupied molecular orbital
hp	horsepower (745.7W)
IB	intermediate band
IEA	International Energy Agency
in	inch (2.54cm)
IPCE	incident photon-to-current conversion efficiency
IQE	internal quantum efficiency
IR	infrared
ISES	International Solar Energy Society
ITO	indium tin oxide
kcal	kilocalorie (4184 joules)
lb	pound (0.454kg)
LBSF	local back surface field
LCP	laser chemical processing
LFC	laser-fired contacts
LP	low pressure
LUMO	lowest unoccupied molecular orbital
ly	langley (1ly/min = 697.5W/m ²)
MEG	multiple exciton generation
MIS	metal insulator conductor
MIT	Massachusetts Institute of Technology
MOCVD	metal-organic chemical vapour deposition
NC	nanocrystal
nc	nanocrystalline
NMR	nuclear magnetic resonance
NSF	National Science Foundation
P3HT	poly-3(hexylthiophene)
PCE	power conversion efficiency
PECVD	plasma-enhanced chemical vapour deposition
PEDOT:PSS	poly(3,4-ethylenedioxythiophene) poly(styrenesulphonate)
PERC	passivated emitter and rear cell
POC	proof of concept
ppmv	parts per million by volume
PV	photovoltaic(s)
QD	quantum dot

QY	quantum yield
R&D	research and development
RANN	Research Applied to National Needs (NSF)
RF	radio frequency
RTSE	real-time spectroscopic ellipsometry
SEGS	solar electric generation system
SQ	Shockley and Queisser
SRH	Shockley–Read–Hall
SS	stainless-steel substrate
st	steradian
SWE	Staebler-Wronski effect
TCO	transparent conducting oxide
TDDFT	time-dependent density functional theory
TFT	thin-film transistor
TOP/TOPO	trioctylphosphine and trioctylphosphine oxide
TPD	N,N'-diphenyl-N,N'-bis(3-methylphenyl) (1,1'-biphenyl-4,4'-diamine)
UV	ultraviolet
VB	valence band
VHF	very high frequency
μc	microcrystalline
Ω/sq	ohms per square (sheet resistance)

Contents

<i>List of figures, tables and boxes</i>	<i>ix</i>
<i>List of abbreviations</i>	<i>xxvii</i>

Volume II: Editorial Introduction	1
<i>Bent Sørensen</i>	

Part I Solar Electricity

1 Photovoltaic Effect of p-n Junctions in Germanium	15
<i>M. Becker and H. Y. Fan</i>	
2 Photovoltaic Effect in p-n Junctions	18
<i>Robert L. Cummerow</i>	
3 Photovoltaic Effect in GaAs p-n Junctions and Solar Energy Conversion	31
<i>D. A. Jenny, J. J. Loferski and P. Rappaport</i>	
4 Detailed Balance Limit of Efficiency of p-n Junction Solar Cells	35
<i>William Shockley and Hans Queisser</i>	
5 Increasing the Efficiency of Ideal Solar Cells by Photon-Induced Transitions at Intermediate Levels	55
<i>Antonio Luque and Antonio Martí</i>	
6 Solar Cell Efficiency Tables (Version 22)	63
<i>Martin A. Green, Keith Emery, David L. King, Sanekazu Igari and Wilhelm Warta</i>	
7 Theory of the Electrical and PV Properties of Polycrystalline Silicon	72
<i>Amal K. Ghosh, Charles Fishman and Tom Feng</i>	
8 Improved Modelling of Grain Boundary Recombination in Bulk and p-n Junction Regions of Polycrystalline Silicon Solar Cells	92
<i>S. A. Edmiston, G. Heiser, A. B. Sproul and M. A. Green</i>	

9	Very High-Efficiency Solar Cell Modules <i>Allen Barnett et al</i>	114
10	High-Efficiency Solar Cells on Phosphorus Gettered Multicrystalline Silicon Substrates <i>O. Schultz, S. W. Glunz, S. Riepe and G. P. Willeke</i>	129
11	Analysis of Ultrathin High-Efficiency Silicon Solar Cells <i>Daniel Kray and Keith R. McIntosh</i>	140
12	Solar Cells from Colloidal Nanocrystals: Fundamentals, Materials, Devices and Economics <i>Hugh W. Hillhouse and Matthew C. Beard</i>	152
13	Substitutional Doping of Amorphous Silicon <i>W. E. Spear and P. G. Le Comber</i>	186
14	A New Type of Amorphous Silicon Photovoltaic Cell Generating More than 2.0V <i>Y. Hamakawa, H. Okamoto and Y. Nitta</i>	191
15	Thin-Film Si:H-Based Solar Cells <i>C. R. Wronski, B. Von Roedern and A. Kolodziej</i>	195
16	Dye-Sensitized Zinc Oxide: Aqueous Electrolyte: Platinum Photocell <i>H. Tsubomura, M. Matsumura, Y. Nomura and T. Amamiya</i>	205
17	A Low-Cost, High-Efficiency Solar Cell Based on Dye-Sensitized Colloidal TiO₂ Films <i>Brian O'Regan and Michael Grätzel</i>	208
18	A Coumarin-Derivative Dye-Sensitized Nanocrystalline TiO₂ Solar Cell Having a High Solar Energy Conversion Efficiency up to 5.6 Per Cent <i>Kohjiro Hara, Kazuhiro Sayama, Yasuyo Ohga, Akira Shinpo, Sadaharu Suga and Hironori Arakawa</i>	214
19	Surface Reactions in Photoelectrochemical Cells <i>Bent Sørensen</i>	219

20	Combined Experimental and DFT-TDDFT Computational Study of Photoelectrochemical Cell Ruthenium Sensitizers	227
	<i>Mohammad K. Nazeeruddin, Filippo De Angelis, Simona Fantacci, Annabella Selloni, Guido Viscardi, Paul Liska, Seigo Ito, Bessho Takeru and Michael Grätzel</i>	
21	Analytical Design of Antireflection Coatings for Silicon Photovoltaic Devices	252
	<i>P. Nubile</i>	
22	Effect of Temperature on Photovoltaic Solar Energy Conversion	261
	<i>Joseph J. Wysocki and Paul Rappaport</i>	
23	Hydrogen-Evolving Solar Cells	275
	<i>Adam Heller</i>	
24	Innovative Renewable Energy Solutions for Hydrogen Vehicles	293
	<i>Haruki Tsuchiya</i>	
25	Thin-Film Silicon Photovoltaics: Architectural Perspectives and Technological Issues	305
	<i>Lucia Vittoria Mercaldo, Maria Luisa Addonizio, Marco Della Noce, Paola Delli Veneri, Alessandra Scognamiglio and Carlo Privato</i>	

Part II Solar Heat

26	The Performance of Flat-Plate Solar Heat Collectors	325
	<i>H. C. Hottel and B. B. Woertz</i>	
27	The Performance of an Experimental System Using Solar Energy for Heating and Night Radiation for Cooling a Building	356
	<i>Raymond W. Bliss, Jr.</i>	
28	Solar Heating and Cooling	371
	<i>John A. Duffie and William A. Beckman</i>	
29	Calculation of Flat-Plate Collector Loss Coefficients	387
	<i>S. A. Klein</i>	
30	Results of Solar Heating Experiments	392
	<i>B. J. Brinkworth</i>	

31	Report on Two and a Half Years' Experimental Living in Yanagimachi Solar House II <i>Masanosuke Yanagimachi</i>	407
32	Solar Heat Systems for Use at High Latitudes <i>Bent Sørensen</i>	428
33	Design and Construction of a Residential Solar Heating and Cooling System <i>Dan S. Ward and George O. G. Löf</i>	435
34	Ninety Metal Drums Collect and Store Heat <i>L. Gropp</i>	449
35	German Central Solar Heating Plants with Seasonal Heat Storage <i>D. Bauer, R. Marx, J. Nußbicker-Lux, F. Ochs, W. Heidemann and H. Müller-Steinhagen</i>	455
36	Ideal Light Concentrators with Reflector Gaps <i>R. Winston</i>	474
37	1000kW Solar Furnace Built by the National Center of Scientific Research in Odeillo, France <i>Felix Trombe and Albert le Phat Vinh</i>	478
38	First Results Obtained with the 1000kW Solar Furnace <i>Felix Trombe, Leon Gion, Claude Royere and Jean Francois Robert</i>	483
39	Modelling of Parabolic Trough Direct Steam Generation Solar Collectors <i>S. D. Odeh, G. L. Morrison and M. Behnia</i>	487
40	Practical Solar Cooking Ovens <i>Maria Telkes and Stella Andrassy</i>	507
41	Solar Ponds: Large-Area Solar Collectors for Power Production <i>H. Tabor</i>	517
42	Solar Energy, Building and the Law <i>Ralph Knowles</i>	529
	<i>Index</i>	541

List of Figures, Tables and Boxes

Figures

II.1	First page of Edmond Becquerel's paper on solar cells from 1839	2
II.2	First page of 1887 paper by James Moser on the dye-sensitized solar cell	5
1.1	Effect of external load resistance on photovoltage	15
1.2	Photovoltage as a function of light intensity	16
1.3	Temperature dependence of spectral response	16
2.1	Energy levels for electrons and the electrostatic potential in the transition region of a $p-n$ junction	18
2.2	Model of $p-n$ junction used for calculations	20
2.3	Efficiency of power conversion as a function of the distance from electrode to junction	26
2.4	Efficiency of power conversion as a function of power input for 1 ohm-cm germanium at 300K, $d = 2.5 \times 10^{-3}$ cm	26
2.5	Efficiency of power conversion as a function of power input for 0.01 ohm-cm germanium for three different temperatures, $d = 3.5 \times 10^{-3}$ cm	27
3.1	Comparison of theoretical $i-V$ curve with experimental points obtained from solar illumination on a GaAs $p-n$ junction	32
3.2	Spectral response of GaAs photovoltaic $p-n$ junction	33
4.1	Comparison of the 'semi-empirical limit' of efficiency of solar cells with the 'detailed balance limit' derived in this chapter	36
4.2	Schematic representation of the solar battery considered: (a) a spherical solar battery surrounded by a black body of temperature T_s ; the solar battery is at temperature $T_c = 0$; (b) a planar cell irradiated by a spherical sun subtending a solid angle ω_s at angle of incidence θ	38
4.3	Dependence of the ultimate efficiency $\eta(x_g)$ upon the energy gap V_g of the semiconductor	40
4.4	Relationship between the impedance matching factor m and the open circuit voltage of a solar cell	46

4.5	Efficiency η for a black-body solar cell at $T_c = 300\text{K}$, with sun at $T_s = 6000^\circ\text{C}$, as a function of energy gap for different values of the parameter f	48
4.6	Efficiency η for a solar cell at temperature $T_c = 300\text{K}$ exposed to a black-body sun at temperature $T_s = 6000\text{K}$	48
4.7	Current–voltage relationships at room temperature for silicon p – n junctions used as solar energy converters	49
5.1	Band diagram of a solar cell with an intermediate band	56
5.2	Efficiency limit for a solar cell with an intermediate band and for a two-terminal ideal tandem cell, in both cases vs. the lowest band gap ϵ_1 , and for a cell with a single band gap	59
5.3	Band diagram of a two-terminal tandem cell	60
7.1	Efficiency versus grain size	73
7.2	Grain boundaries at different physical locations within a solar cell	73
7.3	Average free-carrier concentration and mobility as a function of doping density in polycrystalline silicon	74
7.4	Mobility–minimum doping density versus grain size	75
7.5	Resistivity versus doping concentration of polycrystalline silicon as compared with single-crystal results	75
7.6	Mobility versus grain size	76
7.7	Lifetime versus grain size	79
7.8	Diffusion length as a function of grain size	79
7.9	Reverse saturation current J_{or} (due to recombination) as a function of grain size	81
7.10	Short-circuit photocurrent versus diffusion length	83
7.11	Short-circuit photocurrent versus diffusion length	83
7.12	Effect of barrier shrinkage and mobility on J_{sc}	84
7.13	Effect of thickness on short-circuit photocurrent	86
7.14	Effect of grain size on V_{oc}	87
7.15	Effect of grain size on fill factor	87
7.16	Effect of grain size on efficiency with and without barrier shrinkage.	88
7.17	Effect of grain size on efficiency at different thicknesses t	88
7.18	Grain size and thickness relationship for 10 and 11 per cent efficiency cells	89
8.1	Device geometries used in the simulation of (a) horizontal and (b) vertical grain boundaries	98
8.2	Recombination current vs. voltage for a horizontal grain boundary in a quasi-neutral region in 10^{16}cm^{-3} doped polysilicon for grain boundaries with trap state densities of (a) 10^{12} and (b) 10^{11}cm^{-3}	100

8.3	Effective surface recombination velocity for a horizontal grain boundary as a function of device voltage for 10^{16}cm^{-3} doped polysilicon for grain boundaries with trap state densities of (a) 10^{12} and (b) 10^{11}cm^{-3}	101
8.4	Numerical and semi-analytical models for (a) the peak vertical electric field within a $p-n$ junction far from a grain boundary, (b) the peak vertical electric field within a $p-n$ junction at a grain boundary, and (c) the disturbance to the vertical electric field caused by the grain boundary	104
8.5	Recombination current density at a vertical grain boundary within the $p-n$ junction depletion region for (a) 10^{16}cm^{-3} doped silicon, trap state density $N_t = 10^{12}\text{cm}^{-2}$ ($S = 2 \times 10^4\text{cm/s}$) and (b) 10^{18}cm^{-3} doped silicon, trap state density $N_t = 10^{13}\text{cm}^{-2}$ ($S = 2 \times 10^5\text{cm/s}$)	105
8.6	Electric field and recombination rate in the plane of a grain boundary, perpendicular to the $p-n$ junction.	106
8.7	Saturation current density and ideality factor for recombination arising solely at the grain boundary in the vicinity of a $p-n$ junction as a function of the surface recombination velocity at the grain boundary	108
8.8	Recombination current density at a vertical grain boundary outside of the $p-n$ junction depletion region as a function of device voltage for two different trap state densities	110
8.9	Hole current flow within a grain containing a vertical grain boundary at open circuit	111
9.1	Schematic showing the optical elements in the lateral optics, including a static concentrator and spectral splitting	115
9.2	Schematic of the solar system architecture, which combines new optical elements	116
9.3	Schematic of the fabricated POC	117
9.4	Assembled crossed cylinders POC	118
9.5	Optical transmission as a function of angle away from normal to the module	118
9.6	Performance of the POC with east/west tracking angle	119
9.7	Predicted contributions of each solar cell in the proposed six-junction design	121
9.8	Typical $I-V$ curve for a GaN/InGaN solar cell with semi-transparent p -contact metal	122
9.9	$I-V$ curve of the best GaInP/GaAs solar cell at $20\times$	123
9.10	Cell design in millimetres	124

9.11	Best silicon solar cell under idealized GaAs filter at 8.7×	125
9.12	I - V data for the top and bottom sub-cells of a three-terminal GaInAsP/GaInAs tandem cell 42× suns under an idealized Si filter	126
10.1	High-efficiency solar cell structure for multicrystalline silicon	131
10.2	Process flow for high-efficiency solar cells produced in this study	132
10.3	In the thermally non-treated sample the minority-carrier lifetime is correlated with the dislocation density	133
10.4	After a phosphorus diffusion at 880°C, the minority-carrier lifetime of a wafer adjacent to the reference wafer is increased	133
10.5	Photograph of eight adjacent solar cells of 1 cm ² and a half cell of 4 cm ² on one wafer	135
10.6	A microscopic model was used to quantitatively describe the dependence of the effective carrier lifetime on dislocation density under the assumption of a recombination strength Γ and a carrier lifetime $\tau_{\text{background}}$	136
10.7	Measured data and calculated fit of carrier lifetime dependence on dislocation density for the reference wafer and a phosphorus-diffused wafer	137
10.8	After a POCl ₃ diffusion for 90 minutes at 880°C the minority-carrier lifetime increased by a factor of three in lightly dislocated regions, whereas in highly dislocated areas only a small effect was observed	137
11.1	Important scales in 40 μm thin cells	142
11.2	Measured modelled bulk series resistance for solar cells with different thicknesses	143
11.3	Extracted front series resistance contribution for different LFC pitches and cell thicknesses	144
11.4	Simulated and measured V_{oc} of solar cells on different materials with varying thickness and LFC contact pitch	145
11.5	Local ideality factor at V_{oc} for cells on 0.5 Ω cm FZ(B) with different thickness	146
11.6	Measured FF loss due to series resistance plotted versus the cell thickness and the series resistance	147
11.7	Measured and simulated FF for different cell thickness and base material	148
11.8	Simulation results of dark saturation current densities and respective implied V_{oc} for solar cells with varying thickness on good and medium quality substrate material	149
11.9	Analytical calculations of solar cell efficiencies for varying base material, cell thickness and contact pitch	150
12.1	The cost of electrical power from photovoltaic systems is shown as a function of the total up-front cost and the module power conversion efficiency	154

12.2	Theoretical limit of efficiency for solar cells that utilize MEG but otherwise obey the same physics as the Shockley–Queisser balance calculation: (a) several possible quantum yield profiles and (b) resulting theoretical efficiency	156
12.3	Electronically coupled NCs that reside within a built-in electric field (E) suitable for device operation	161
12.4	Schottky-junction NC solar cell	166
12.5	Hybrid semiconductor nanocrystal and amorphous silicon PV device	168
12.6	Heterojunction photovoltaic device using printed colloidal quantum dots	169
12.7	Copper(I) sulphide nanocrystals and resulting solar cells on flexible substrates	174
12.8	CuInSe ₂ solar cells fabricated from a nanocrystal ink	176
13.1	The effect of phosphorus and boron doping on the conductivity and the position of the Fermi level in a-Si specimens	187
14.1	Schematic representations for the principle of the device: (a) device construction, (b) band diagram in the dark, (c) band diagram under illumination, (d) equivalent circuit	192
14.2	An explanation of the optimum design rule for the unit-cell thickness in the device	193
14.3	Open-circuit voltage V_{oc} , short-circuit current density J_{sc} , and cell efficiency η as a function of the number of $p-i-n$ unit cells m under the 80mW/cm ² sunlight	194
15.1	Schematic of the structure of Si:H films prepared as a function of R	197
15.2	Light $I-V$ characteristics of the customized $p-i-n$ solar cells fabricated with the two-step i -layer having different thickness p/i interface layers	198
15.3	$2 \times 2\mu\text{m}$ AFM images of the $R = 40$ Si:H films at the same thickness used in the customized cell structures	199
15.4	Extended phase diagram for p-Si:H deposited on protocrystalline a-Si:H as a function of R and thickness. Also shown is the 1 sun V_{oc} for cell structures with corresponding $\sim 200\text{\AA}$ p -layers	200
15.5	Fill factor under 1 sun illumination at 25°C for $p-i-n$ solar cells with 400nm i -layers deposited with $R = 0$ and $R = 10$ at 200°C as well as changes in the forward bias current in an a-Si:H cell and the reciprocal of the current in the corresponding film for a carrier generation rate of $2 \times 10^{16}\text{cm}^{-2}\text{ s}^{-1}$	201
16.1	The design of the photocell	206
16.2	Curve of photocurrent (i_{ph}) against photovoltage (V_{ph}) for the ZnO photocell dyed with rose bengal	206

17.1	Schematic representation of the principle of the dye-sensitized photovoltaic cell to indicate the electron energy level in the different phases	209
17.2	Transmission electron micrograph of TiO ₂ particles used in thin film production	210
17.3	Absorption and photocurrent action spectra of TiO ₂ films supported on conducting glass	211
17.4	Photocurrent–voltage characteristics of a cell, based on a colloidal TiO ₂ film sensitized by 1 ; the film, supported on a conducting glass sheet, was used in a sandwich-type configuration	212
18.1	Molecular structure of new coumarin derivatives.	215
18.2	Absorption spectra of C343, 1 and 2 in EtOH, and of 2 adsorbed on a TiO ₂ film whose absorbance is normalized	216
18.3	Typical action spectra of incident photon-to-current conversion efficiencies (IPCE) obtained for nanocrystalline TiO ₂ solar cells sensitized by 2 and Ru(dcbpy) ₂ (NCS) ₂ (TBA) ₂	217
19.1	Block of anatase with coumarin-derivative dye molecule	220
19.2	Simplified model used for initial exploration, with only one layer of anatase	221
19.3	Result of applying unrestricted optimization of the position of all atoms to the simplified structure of Figure 19.2	221
19.4	Initial structure used for the final, restricted optimization	222
19.5	Final results of realistically restricted optimization: (a) seen from the same angle as Figure 19.4, and (b) seen from the ‘end’ of the anatase wavy lines connecting atoms in (a)	223
19.6	Electron density difference between excited and ground state of coumarin-derivative dye	223
19.7	Electron density difference between first excited and ground states, calculated for the coumarin-based dye molecule using the ZINDO approximation	225
19.8	Electron density difference between first excited and ground states, calculated for the coumarin-based dye molecule using a Hartree-Fock calculation	225
19.9	Electron density difference between first excited and ground states, calculated as the difference between LUMO and HOMO densities from the same B3LYP calculation as Figures 19.6 and 19.10	226
19.10	Electron density difference between first excited and ground states, calculated using the density functional theory B3LYP method as in Figure 19.6, and a large orbital basis called 6-311+G(d,p)	226
20.1	Optimized molecular structures of the N719 (a–c isomers), N621 and of the fully protonated and fully deprotonated N3 complexes	229